Original Article

Value of spectral computed tomography-derived quantitative parameters based on full volume analysis in the diagnosis of benign/malignant and pathological subtypes of solitary pulmonary nodules

Kaifang Liu[1#], Meiqin Wang[1#], Youtao Xu[2], Qing Chen[1], Kang Li[1], Lei Zhang[1], Xiaodong Xie[1], Wenrong Shen[1]

[1]Department of Radiology, Jiangsu Cancer Hospital, Jiangsu Institute of Cancer Research, Nanjing Medical University Affiliated Cancer Hospital, Nanjing, China; [2]Department of Thoracic Surgery, Jiangsu Cancer Hospital, Jiangsu Institute of Cancer Research, Nanjing Medical University Affiliated Cancer Hospital, Nanjing, China

Contributions: (I) Conception and design: X Xie, W Shen; (II) Administrative support: M Wang, W Shen; (III) Provision of study materials or patients: K Liu, Y Xu, M Wang; (IV) Collection and assembly of data: K Liu, M Wang, X Xie, Y Xu, Q Chen, K Li, L Zhang; (V) Data analysis and interpretation: X Xie, K Liu, M Wang, Y Xu, Q Chen, K Li; (VI) Manuscript writing: All authors; (VII) Final approval of manuscript: All authors.

[#]These authors contributed equally to this work.

Correspondence to: Xiaodong Xie; Wenrong Shen. Department of Radiology, Jiangsu Cancer Hospital, Jiangsu Institute of Cancer Research, Nanjing Medical University Affiliated Cancer Hospital, 42 Baiziting Road, Nanjing 210000, China. Email: xiaodong8196@126.com; jszlyyct@126.com.

Background: Conventional dynamic computed tomography (CT) has a low specificity for the distinction between benign and malignant solitary pulmonary nodules (SPNs), and spectral CT has been proposed as a potential alternative. We aimed to investigate the role of quantitative parameters based on full-volume spectral CT in the differential diagnosis of SPNs.

Methods: This retrospective study included spectral CT images of 100 patients with pathologically confirmed SPNs (78 and 22 in the malignant and benign groups, respectively). All cases were confirmed by postoperative pathology, percutaneous biopsy, and bronchoscopic biopsy. Multiple quantitative parameters derived from spectral CT were extracted from whole-tumor volume and standardized. Differences in quantitative parameters between groups were statistically analyzed. Diagnostic efficiency was evaluated by generating a receiver operating characteristic (ROC) curve. Between-group differences were evaluated using an independent sample *t*-test or Mann-Whitney U test. Interobserver repeatability was assessed using intraclass correlation coefficients (ICCs) and Bland-Altman plots.

Results: Spectral CT-derived quantitative parameters, except attenuation difference between the SPN in the 70 keV and arterial enhancement [$\Delta_{S\text{-}A(70\ keV)}$], were significantly higher for malignant SPNs than for benign nodules (P<0.05). In the subgroup analysis, most parameters could distinguish between the benign and adenocarcinoma groups, and between the benign and squamous cell carcinoma groups (P<0.05). Only 1 parameter could differentiate the adenocarcinoma and squamous cell carcinoma groups (P=0.020). ROC curve analysis indicated that normalized arterial enhancement fraction in the 70 keV ($NEF_{70\ keV}$), normalized iodine concentration (NIC), and Δ70 keV had high diagnostic efficacy for differentiating SPNs between the benign and malignant SPNs [area under the curve (AUC): 0.867, 0.866, and 0.848, respectively] and between the benign and adenocarcinoma groups (AUC: 0.873, 0.872, and 0.874, respectively). The multiparameters derived from spectral CT exhibited satisfactory interobserver repeatability (ICC: 0.856–0.996).

Conclusions: Our study suggests that quantitative parameters derived from whole-volume spectral CT may be useful to improve discrimination of SPNs.

Keywords: Spectral computed tomography (spectral CT); full-volume analysis; quantitative parameters; solitary pulmonary nodules (SPNs)

Submitted Sep 18, 2022. Accepted for publication Mar 30, 2023. Published online Apr 12, 2023.
doi: 10.21037/qims-22-979
View this article at: https://dx.doi.org/10.21037/qims-22-979

Introduction

Lung cancer (LC) is the leading cause of cancer-related deaths, with increasing morbidity and mortality worldwide (1,2). As many early-stage LCs are asymptomatic, the greatest opportunity for cure is often missed, and LCs are typically detected at an advanced stage. Early-stage LC manifests predominantly as a solitary pulmonary nodule (SPN), which can be surgically removed to improve survival (3). SPN is defined as a round or oval shadow with a diameter ≤3 cm that is completely surrounded by the pulmonary parenchyma and without other abnormalities (4-6). Previous studies have reported that the prevalence of malignant tumors in patients with SPN ranges from 10% to 70% (7-9). Low-dose computed tomography (CT) is the best screening method for LC and can reduce the death rate from LC by 20% (10). Nevertheless, the qualitative diagnosis of SPNs remains an ongoing diagnostic challenge. Therefore, timely and reliable differentiation of SPNs is crucial for guiding treatment plans and prognosis of patients.

Conventional CT plays an important role in evaluating the imaging signs and enhancement features of SPN, but some benign and malignant SPN have highly similar lesion morphology and enhancement patterns, so it remains a great challenge to distinguish between benign and malignant SPNs (11,12). Spectral CT recently emerged as a considerable advance in the field of CT. Spectral CT imaging is based on multisubstance decomposition algorithm techniques, which can extract the iodine concentration (IC), slope of the spectral decay curve, and effective atomic number (Zeff), to reflect information on tumor angiogenesis and microenvironment. This approach is being increasingly used clinically and has high diagnostic accuracy for many organ diseases (13). Several studies have demonstrated that spectral CT has potential value for distinguishing benign and malignant lung lesions, tissue subtypes, and lymphatic metastases (14-18). However, most previous studies (14-18) have obtained the various parameters from regions of interest (ROIs) drawn manually on the largest lesion slices. This may lead to measurement sampling bias, which is often the only parameter used and cannot reflect information on the tissue characteristics of the entire lesion and, therefore, cannot adequately assess intralesional heterogeneity. A recent radiology study reported that nodule volumes obtained using a semiautomated CT volume method showed greater interobserver agreement, less variability, and improved reproducibility of quantitative analysis compared to manual or semiautomated nodule diameters (19).

To the best of our knowledge, the role of spectral CT-derived multiparameter quantification combined with full-volume analysis for distinguishing SPNs is yet to be reported. This study aimed to evaluate the potential of spectral CT-derived multiparameters based on full-volume acquisition for the differentiation of benign and malignant SPNs. We present the following article in accordance with the STARD reporting checklist (available at https://qims.amegroups.com/article/view/10.21037/qims-22-979/rc).

Methods

Ethics

The study was conducted in accordance with the Declaration of Helsinki (as revised in 2013). The Institutional Ethics Committee of Jiangsu Cancer Hospital approved this study, and individual consent for this retrospective analysis was waived.

Patients

Between September 2021 and May 2022, 124 patients with clinically diagnosed SPNs were enrolled. The inclusion criteria were as follows: (I) suspected SPNs, (II) underwent spectral CT chest-enhanced scan at our hospital, and (III) confirmation by pathology. All cases were confirmed by postoperative pathology, percutaneous biopsy, and bronchial biopsy. The exclusion criteria were as follows: (I) lesion diameter was ≥3.0 cm and ≤0.8 cm (n=14), (II) patients with more than 1 nodule (n=2), (III) clinical treatment before CT examination (n=2), (IV) nonsolid pulmonary nodules (n=3),

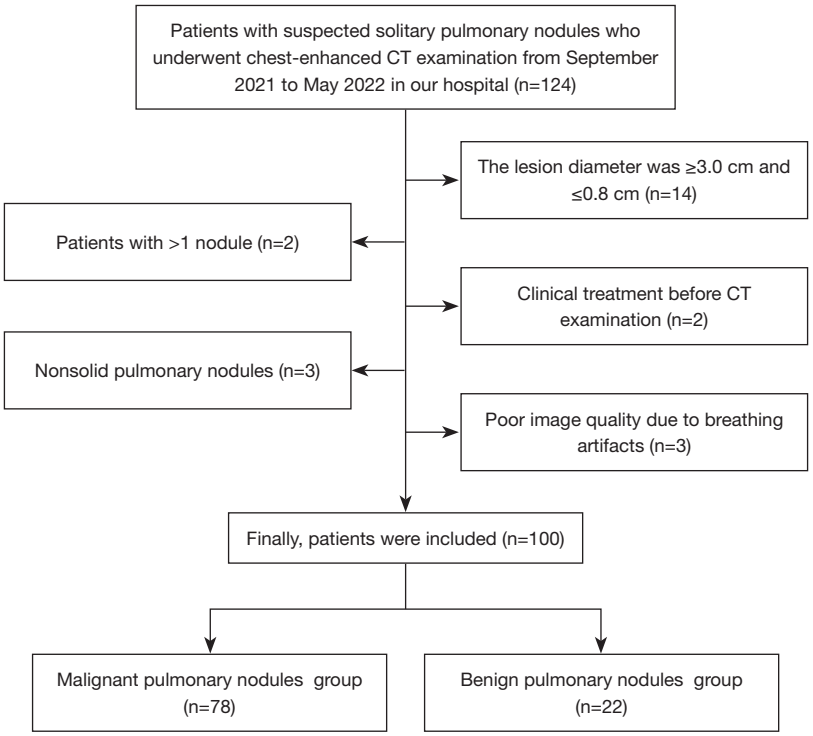

Figure 1 Patients enrolment flowchart. CT, computed tomography.

and (V) poor imaging quality due to respiratory artifacts (n=3). The patient selection flowchart is presented in *Figure 1*.

We collected and analyzed the data of 100 patients. Among these, 68 cases were confirmed by postoperative pathology, 29 cases by percutaneous biopsy, and 3 cases by bronchoscopic biopsy. Based on the pathological results, the patients were divided into benign, malignant, adenocarcinoma, and squamous cell carcinoma groups for statistical analysis. The cases comprised 22 benign pulmonary nodules (inflammation, n=11; hamartoma, n=5; tuberculosis, n=4; inflammatory pseudotumor, n=2) and 78 malignant pulmonary nodules (adenocarcinoma, n=60; squamous cell carcinoma, n=14; small cell LC, n=2; atypical carcinoid, n=1; and adenosquamous carcinoma, n=1).

CT image acquisition

All patients underwent the same routine protocol using dual-layer spectral CT (IQon; Philips Healthcare, Best, Netherlands). Patients were positioned in the supine position, and the scanning range was from the thoracic entrance to the level of the costophrenic angle. The scanning parameters were as follows: tube voltage, 120 kVp; tube current modulation, three-dimensional (3D) modulation; collimator width, 64×0.625 mm^2; matrix, 512×512; scanning field of view, 372 mm; spacing, 0.90; rotation time, 0.50 s; scanning slice thickness, 5 mm; and reconstruction slice thickness, 1 mm. Contrast agent (ioversol, 3.0 mL/kg; iodine, 350 mg/mL; HengRui Medicine, Jiangsu, China) was injected into the antecubital vein at a flow rate of 3 mL/s, followed by a follow-up injection of 20 mL of normal saline at the same flow rate. A chest enhancement scan was performed 50 seconds after completion.

Image analysis

Images were imported into a Philips workstation (IntelliSpace Portal; Philips Healthcare) for analysis and processing using the 3D semiautomatic segmentation workstation's own software (Tumor Tracking, Multimodality). Image analysis was performed by a radiologist (LKF, 4 years of radiology experience) and supervised by a senior radiologist (XXD, 8 years of radiology experience), who were blind to the clinicopathological information. All images were acquired in the mediastinal window, and the lesions were identified by reading the images. ROIs of the pulmonary nodules were automatically segmented with the software and

underwent normalization processing. Subsequently, a series of parameters were obtained, as follows: CT value of solitary pulmonary nodule at virtual noncontrast was recorded as $CT_{SPN\text{-}VNC}$; enhancement (40 and 70 keV) values were recorded as $CT_{SPN\text{-}40\ keV}$ and $CT_{SPN\text{-}70\ keV}$, respectively; virtual noncontrast of aorta and CT mean of 70 keV were recorded as $CT_{aorta\text{-}VNC}$ and CT_{aorta}, respectively. The CT values of virtual plain scans and the aorta were used as a reference. The difference between CT values of the lesion after enhancement and virtual plain scans ($\Delta_{40\ keV}$ and $\Delta_{70\ keV}$), difference between the lesion and aorta ($\Delta_{S\text{-}A}$), and contrast enhancement ratio were calculated using the following formulas ($CER_{40\ keV}$ and $CER_{70\ keV}$), SPN to arterial enhancement ratio ($SAR_{40\ keV}$ and $SAR_{70\ keV}$) (20-22), normalized arterial enhancement fraction ($NEF_{40\ keV}$ and $NEF_{70\ keV}$), and spectral curve slope (λ) (23,24).

$$\Delta_{40\ keV/70\ keV} = CT_{SPN\text{-}40\ keV/70\ keV} - CT_{SPN\text{-}VNC} \quad [1]$$

$$\Delta_{S\text{-}A(40\ keV/70\ keV)} = CT_{SPN\text{-}40\ keV/70\ keV} - CT_{aorta} \quad [2]$$

$$CER_{40\ keV/70\ keV} = \Delta_{40\ keV/70\ keV} / CT_{SPN\text{-}VNC} \quad [3]$$

$$SAR_{40\ keV/70\ keV} = CT_{SPN\text{-}40\ keV/70\ keV} / CT_{aorta} \quad [4]$$

$$NEF_{40\ keV/70\ keV} = \Delta_{40\ keV/70\ keV} / \left(CT_{aorta} - CT_{aorta\text{-}VNC}\right) \quad [5]$$

$$\lambda = \left(CT_{SPN\text{-}40\ keV} - CT_{SPN\text{-}70\ keV}\right) / \left(70 - 40\right) \quad [6]$$

To account for hemodynamic changes between patients, the IC (mg/mL) and Zeff values were normalized to those of the aorta. The normalized Zeff (NZeff) and normalized IC (NIC) were calculated using the following formulas (25-27):

$$NZeff = Z_{SPN} / Z_{aorta} \quad [7]$$

$$NIC = IC_{SPN} / IC_{aorta} \quad [8]$$

To assess interobserver repeatability and variability, 50% of the study participants (50 of 100) were randomly selected, and previous measurement procedures were repeated by an additional physician (WMQ, 14 years of radiology experience). Interobserver agreement was assessed using Bland-Altman plots and intraclass correlation coefficients (ICCs).

Statistical analysis

Data were statistically analyzed using the software SPSS 22.0 (IBM Corp., Armonk, NY, USA) and MedCalc15 (MedCalc Software, Mariakerke, Belgium). Continuous variables were expressed as means ± standard deviations. Normality was assessed using the Kolmogorov-Smirnov method, followed by testing for homogeneity of variances using the Levene's test. Parameters derived from spectral CT of pulmonary nodules were compared between the two groups using an independent samples *t*-test or Mann-Whitney U test, as appropriate. Receiver operating characteristic (ROC) curve analysis was performed to determine the area under the curve (AUC), accuracy, sensitivity, and specificity. Interobserver agreement for parameters related to CT values was estimated using ICCs (0.000–0.200: poor; 0.201–0.400: fair; 0.401–0.600: moderate; 0.601–0.800: good; 0.801–1.000: excellent). Bland-Altman plot assessment was also performed. Statistical tests were two-tailed, and P<0.05 was considered significant.

Results

Statistical analysis of basic clinical data of benign and malignant SPNs

A total of 100 patients with pathologically diagnosed SPNs were included in this study, including 22 patients with benign SPNs with an average age of 60.591±8.455 years, 13 males and 9 females; and 78 patients with malignant nodules with an average age of 64.551±9.478 years, 38 males and 40 females. We analyzed the differences in age, gender, diameter, and volume between the benign and malignant SPN groups, and there were no significant statistical differences (P=0.308, 0.390, 0.540, and 0.451, respectively). The details are shown in *Table 1*.

Differences in spectral CT parameters between benign and malignant SPNs

The results of the parameter analysis between the two groups are presented in *Table 2*. With the exception of $\Delta_{S\text{-}A(70\ keV)}$ (P=0.112), significant differences were observed between malignant and benign groups in the 12 other parameters [$\Delta_{40\ keV}$, $\Delta_{70\ keV}$, $\Delta_{S\text{-}A(40\ keV)}$, $CER_{40\ keV}$, $CER_{70\ keV}$, $SAR_{40\ keV}$, $SAR_{70\ keV}$, $NEF_{40\ keV}$, $NEF_{70\ keV}$, λ, NZeff, and NIC] (all P<0.05). Representative examples of benign and malignant SPNs are shown in *Figure 2*.

Differences in spectral CT parameters between benign, adenocarcinoma, and squamous cell carcinoma groups

The results of parameter analysis among the three groups

Table 1 Statistical analysis of basic clinical data of patients

Parameters	Benign SPN (n=22), mean ± SEM	Malignant SPN (n=78), mean ± SEM	P value
Age (years)	60.591±8.455	64.551±9.478	0.308
Gender, n			0.390
Male	13	38	
Female	9	40	
Diameter (cm)	1.450±0.550	1.628±0.584	0.540
Volume (cm^3)	2.138±2.778	2.852±2.793	0.451

P values were obtained using the chi-square test, independent *t*-test or Mann-Whitney U-test. P<0.05 indicates statistical significance. SPN, solitary pulmonary nodule; SEM, standard error of the mean.

Table 2 Statistical description and univariate analysis of spectral CT-related parameters in benign and malignant SPN groups

Parameters	Benign SPN (n=22), mean ± SEM	Malignant SPN (n=78), mean ± SEM	P value
$\Delta_{40\ keV}$ (HU)	101.03±51.85	165.36±46.29	<0.001
$\Delta_{70\ keV}$ (HU)	25.51±15.60	47.99±15.16	<0.001
$\Delta_{S\text{-}A(40\ keV)}$ (HU)	−81.22±53.53	−19.24±56.75	<0.001
$\Delta_{S\text{-}A(70\ keV)}$ (HU)	−156.74±43.95	−136.62±53.96	0.112
$CER_{40\ keV}$	5.30±5.93	6.26±3.17	0.002
$CER_{70\ keV}$	1.42±1.87	1.83±1.04	<0.001
$SAR_{40\ keV}$	0.62±0.25	0.95±0.29	<0.001
$SAR_{70\ keV}$	0.26±0.11	0.38±0.12	<0.001
$NEF_{40\ keV}$	0.61±0.30	1.05±0.41	<0.001
$NEF_{70\ keV}$	0.15±0.08	0.31±0.13	<0.001
λ	2.52±1.23	3.91±1.09	<0.001
NZeff	0.79±0.04	0.82±0.07	0.003
NIC	0.17±0.08	0.31±0.12	<0.001

P values were obtained by independent *t*-test or Mann-Whitney U-test. P<0.05 indicates statistical significance. CT, computed tomography; SPN, solitary pulmonary nodule; SEM, standard error of the mean; $\Delta_{40\ keV/70\ keV}$, attenuation difference of the solitary pulmonary nodule between 40 keV/70 keV and virtual noncontrast; HU, Hounsfield unit; $\Delta_{S\text{-}A(40\ keV/70\ keV)}$, attenuation difference between the solitary pulmonary nodule in the 40 keV/70 keV and arterial enhancement; $CER_{40\ keV/70\ keV}$, contrast enhancement ratio of the 40 keV/70 keV; $SAR_{40\ keV/70\ keV}$, solitary pulmonary nodule in the 40 keV/70 keV to arterial enhancement ratio; $NEF_{40\ keV/70\ keV}$, normalized arterial enhancement fraction in the 40 keV/70 keV; λ, slope of the spectral attenuation curve; NZeff, normalized effective atomic number; NIC, normalized iodine concentration.

of benign, adenocarcinoma, and squamous cell carcinoma are presented in *Table 3*. With the exception of $\Delta_{S\text{-}A\ (70\ keV)}$ (P=0.138), the 12 other parameters ($\Delta_{40\ keV}$, $\Delta_{70\ keV}$, $\Delta_{S\text{-}A(40\ keV)}$, $CER_{40\ keV}$, $CER_{70\ keV}$, $SAR_{40\ keV}$, $SAR_{70\ keV}$, $NEF_{40\ keV}$, $NEF_{70\ keV}$, λ, NZeff, and NIC) were significantly higher in the malignant group than in the benign group (all P<0.05). With the exception of $\Delta_{S\text{-}A(70\ keV)}$, $CER_{40\ keV}$, and $CER_{70\ keV}$ (P=0.204, 0.144, and 0.088, respectively), the 10 remaining parameters [$\Delta_{40\ keV}$, $\Delta_{70\ keV}$, $\Delta_{S\text{-}A(40\ keV)}$, $SAR_{40\ keV}$, $SAR_{70\ keV}$, $NEF_{40\ keV}$, $NEF_{70\ keV}$, λ, NZeff, and NIC] were significantly higher in the squamous cell carcinoma group than in the benign group (all P<0.05). $CER_{70\ keV}$ was significantly higher in the adenocarcinoma group than in the squamous cell carcinoma group (P=0.020). No significant between-group

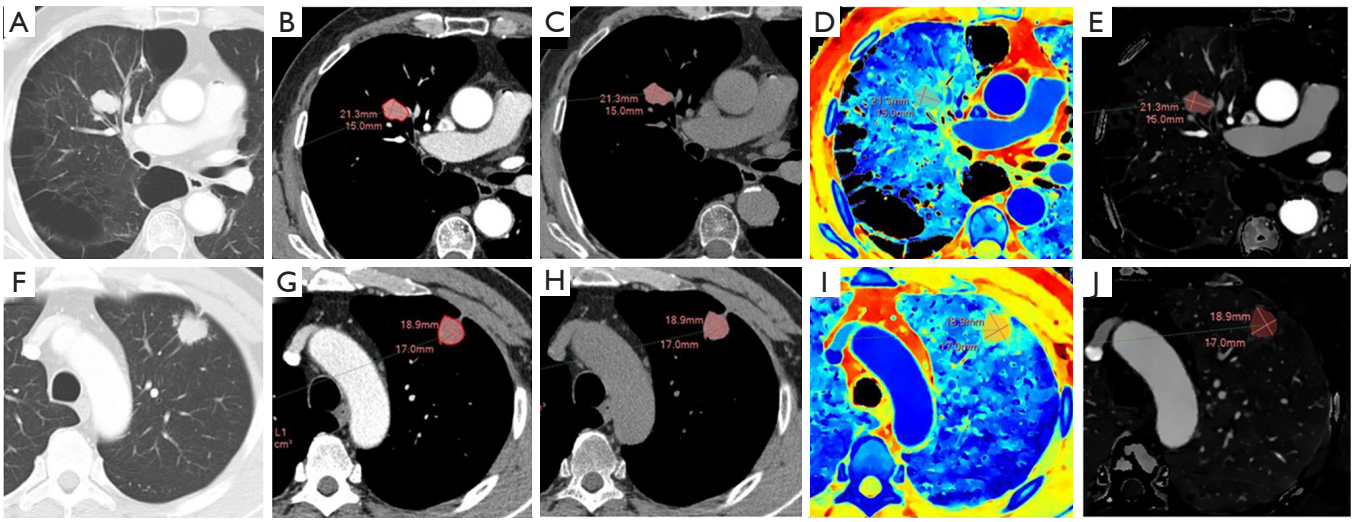

Figure 2 CT images from a 74-year-old man with pathologically confirmed adenocarcinoma of the right upper lobe (A-E) and a 51-year-old woman with pathologically confirmed tuberculosis of the left upper lobe (F-J). From the delineated ROI volume (red), spectral CT of the lesion was obtained for the following quantitative parameters: $CT_{SPN\text{-}70\ keV}$: 98/37; $CT_{SPN\text{-}VNC}$: 33/31; Zeff: 8.7/7.5; IC: 2.6/0.3. CT, computed tomography; ROI, region of interest; $CT_{SPN\text{-}70\ keV}$, CT value of solitary pulmonary nodule at 70 keV; $CT_{SPN\text{-}VNC}$, CT value of solitary pulmonary nodule at virtual noncontrast; Zeff, effective atomic number; IC, iodine concentration.

Table 3 Statistical description and univariate analysis of spectral CT-related parameters in benign, adenocarcinoma, and squamous cell carcinoma groups

Parameters	Benign (n=22)	Adenocarcinoma (n=60)	Squamous cell carcinoma (n=14)	P value		
				Benign *vs.* adenocarcinoma	Benign *vs.* squamous cell carcinoma	Adenocarcinoma *vs.* squamous cell carcinoma
$\Delta_{40\ keV}$ (HU)	101.03±51.85	167.82±42.56	156.66±54.25	<0.001	0.004	0.405
$\Delta_{70\ keV}$ (HU)	25.51±15.60	48.89±13.10	43.44±18.94	<0.001	0.004	0.322
$\Delta_{S\text{-}A(40\ keV)}$ (HU)	−81.22±53.53	−17.76±61.64	−23.41±40.42	<0.001	0.001	0.676
$\Delta_{S\text{-}A(70\ keV)}$ (HU)	−156.74±43.95	−136.69±56.82	−136.64±47.70	0.138	0.204	0.998
$CER_{40\ keV}$	5.30±5.93	6.53±3.29	5.11±1.86	0.001	0.144	0.109
$CER_{70\ keV}$	1.42±1.87	1.92±1.06	1.40±0.63	<0.001	0.088	0.020
$SAR_{40\ keV}$	0.62±0.25	0.97±0.32	0.91±0.20	<0.001	0.001	0.994
$SAR_{70\ keV}$	0.26±0.11	0.39±0.14	0.36±0.09	<0.001	0.002	0.841
$NEF_{40\ keV}$	0.61±0.30	1.08±0.45	0.96±0.25	<0.001	0.001	0.704
$NEF_{70\ keV}$	0.15±0.08	0.32±0.15	0.26±0.09	<0.001	0.001	0.385
λ	2.52±1.23	3.96±1.04	3.77±1.23	<0.001	0.005	0.554
NZeff	0.79±0.04	0.82±0.08	0.82±0.04	0.006	0.020	0.918
NIC	0.17±0.08	0.32±0.13	0.28±0.08	<0.001	0.001	0.508

P values were obtained by independent *t*-test or Mann-Whitney U-test. P<0.05 indicates statistical significance. CT, computed tomography; $\Delta_{40\ keV/70\ keV}$, attenuation difference of the solitary pulmonary nodule between the 40 keV/70 keV and virtual noncontrast; HU, Hounsfield unit; $\Delta_{S\text{-}A(40\ keV/70\ keV)}$, attenuation difference between the solitary pulmonary nodule in the 40 keV/70 keV and arterial enhancement; $CER_{40\ keV/70\ keV}$, contrast enhancement ratio of the 40 keV/70 keV; $SAR_{40\ keV/70\ keV}$, solitary pulmonary nodule in the 40 keV/70 keV to arterial enhancement ratio; $NEF_{40\ keV/70\ keV}$, normalized arterial enhancement fraction in the 40 keV/70 keV; λ, slope of the spectral attenuation curve; NZeff, normalized effective atomic number; NIC, normalized iodine concentration.

differences were noted for the 12 other parameters.

Multiparameter diagnostic performance

The multiparameter diagnostic test characteristics are presented in *Table 4* and *Figure 3*. Among the 12 quantitative parameters that can distinguish between benign and malignant SPN, the AUCs ranged from 0.709 to 0.867, and all of these had high diagnostic efficiency (AUC >0.7). The three quantitative parameters with the highest diagnostic efficacy were $NEF_{70\ keV}$, NIC, and $\Delta_{70\ keV}$, and their AUC were 0.867, 0.866, and 0.848, respectively. Among the 12 quantitative parameters, $NEF_{70\ keV}$ was the highest. When the $NEF_{70\ keV}$ cut-off value was 0.203, the sensitivity was 82.1%, the specificity was 81.8%, and the accuracy was 82.0%. Of the 12 quantitative parameters that could distinguish the benign from the adenocarcinoma groups, the AUCs ranged from 0.699 to 0.874. The three parameters with the highest diagnostic efficacy were $\Delta_{70\ keV}$, $NEF_{70\ keV}$, and NIC, and their AUCs were 0.874, 0.873, and 0.872, respectively. Among the 12 quantitative parameters, $\Delta_{70\ keV}$ was the highest. When the $\Delta_{70\ keV}$ cut-off value was 33.3, the sensitivity, specificity, and accuracy were 93.3%, 72.7%, and 87.8%, respectively. Among the 10 quantitative parameters that differed between the benign and squamous cell carcinoma groups, their AUC ranged from 0.732 to 0.841, and all of these had high diagnostic efficiency (AUC >0.7). The 3 parameters with the highest diagnostic efficacy were NIC, $NEF_{70\ keV}$, and $SAR_{40\ keV}$, and their AUC were 0.841, 0.834, and 0.821, respectively. Among the 10 quantitative parameters, NIC was the highest. When the NIC cut-off value was 0.2, the sensitivity was 92.9%, the specificity 77.3%, and the accuracy 83.3%.

ICCs

All spectral CT-related parameters had good interobserver agreement for assessing lung nodules, with ICC values of 0.856 to 0.996 (*Table 5* and *Figure 4*).

Discussion

This is the first study to demonstrate that CT-derived parameters obtained from spectroscopic CT whole-volume analysis hold potential as reproducible imaging markers for the identification of SPNs. Multiparameter quantitative analyses revealed significant differences in the pulmonary nodules of different pathological types. This approach may help to avoid invasive, time-consuming, and expensive tissue sampling procedures and improve the overall biology of CT scans for characterizing SPNs. These parameters may help to improve discrimination of pulmonary nodule types by radiologists and establish an accurate diagnosis for more effective treatments.

Several studies have demonstrated that the application of enhanced CT-derived CT enhancement values and ratios may reduce the impact of machine and individual differences and may be effective tools for assessing tumor angiogenesis. CT enhancement values and ratios are closely associated with intratumoral microvascular and lymphatic infiltration and can be used as a surrogate marker for preoperative detection of lymphovascular invasion (20,21,28,29).

In the present study, various spectral CT-related parameters were significantly different between benign and malignant pulmonary nodules ($P<0.05$), with the exception of $\Delta_{S\text{-}A(70\ keV)}$ ($P=0.112$). Several derived parameters were significantly higher for malignant pulmonary nodules than for benign pulmonary nodules, which is consistent with previous reports (14,16,30). This may be because malignant nodules produce a large amount of angiogenic factors for tumor growth, which stimulates the formation of more microvessels. The increased density of microvessels leads to an increase in capillary perfusion and permeability, causing rapid accumulation of contrast agent in the interstitium after enhancement. Ultimately, this leads to strong contrast enhancement in malignant nodules.

The spectral curve λ reflects the different X-ray absorption rates of tissues with different chemical compositions. Each tissue has a characteristic spectral curve, which demonstrates the dynamic changes in CT values of different substances with different energy levels. In our study, we demonstrated that the slope (value) of malignant nodules was significantly higher than that of benign nodules. This result is consistent with previous studies (14,16), which can be explained by the following mechanism: a steeper energy spectrum curve is associated with a higher slope value, higher percentage of contrast agent iodine in the tumor, and greater attenuation of iodine at lower energies due to the structural and functional immaturity of the malignant tumor vascular network structure. This results in increased vascular permeability and contrast agent leakage and spectral properties, whereby a stronger curve is associated with a steeper decay curve and higher slope.

Zeff is a quantitative index derived from the atomic number, which represents the compound atoms of

Table 4 Diagnostic performance of different parameters in ROC curve analysis in distinguishing pulmonary nodules

Groups	Parameters	AUC	Cut-off value	Sensitivity, %	Specificity, %	Accuracy, %	P value
Benign *vs.* malignant	$\Delta_{40\ keV}$ (HU)	0.815	120.7	79.5	72.7	78.0	<0.001
	$\Delta_{70\ keV}$ (HU)	0.848	33.3	85.9	72.7	83.0	<0.001
	$\Delta_{S\text{-}A(40\ keV)}$ (HU)	0.785	−63.9	76.9	72.7	76.0	<0.001
	$CER_{40\ keV}$	0.721	3.754	88.5	59.1	82.0	0.004
	$CER_{70\ keV}$	0.771	1.17	80.8	72.7	79.0	<0.001
	$SAR_{40\ keV}$	0.823	0.626	93.6	63.6	87.0	<0.001
	$SAR_{70\ keV}$	0.804	0.339	56.4	95.5	65.0	<0.001
	$NEF_{40\ keV}$	0.832	0.675	91.0	68.2	86.0	<0.001
	$NEF_{70\ keV}$	0.867	0.203	82.1	81.8	82.0	<0.001
	λ	0.793	3.293	70.5	77.3	72.0	<0.001
	NZeff	0.709	0.79	75.6	59.1	72.0	<0.001
	NIC	0.866	0.2	89.7	77.3	87.0	<0.001
Benign *vs.* adenocarcinoma	$\Delta_{40\ keV}$ (HU)	0.833	120.7	83.3	72.7	80.5	<0.001
	$\Delta_{70\ keV}$ (HU)	0.874	33.3	93.3	72.7	87.8	<0.001
	$\Delta_{S\text{-}A(40\ keV)}$ (HU)	0.774	−78	83.3	63.6	78.0	<0.001
	$CER_{40\ keV}$	0.746	3.754	93.3	59.1	84.1	0.001
	$CER_{70\ keV}$	0.800	1.17	90.0	72.7	85.4	<0.001
	$SAR_{40\ keV}$	0.823	0.595	98.3	59.1	87.8	<0.001
	$SAR_{70\ keV}$	0.791	0.339	50.0	95.5	62.2	<0.001
	$NEF_{40\ keV}$	0.836	0.675	90.0	68.2	84.1	<0.001
	$NEF_{70\ keV}$	0.873	0.203	80.0	81.8	80.5	<0.001
	λ	0.807	3.293	75.0	77.3	75.6	<0.001
	NZeff	0.699	0.843	40.0	95.5	54.9	0.001
	NIC	0.872	0.2	88.3	77.3	86.6	<0.001
Benign *vs.* squamous cell carcinoma	$\Delta_{40\ keV}$ (HU)	0.766	120.7	71.4	72.7	72.2	0.001
	$\Delta_{70\ keV}$ (HU)	0.750	27.1	78.6	59.1	66.7	0.003
	$\Delta_{S\text{-}A(40\ keV)}$ (HU)	0.819	−63.9	85.7	72.7	77.8	<0.001
	$SAR_{40\ keV}$	0.821	0.705	92.9	68.2	77.8	<0.001
	$SAR_{70\ keV}$	0.815	0.339	71.4	95.5	86.1	<0.001
	$NEF_{40\ keV}$	0.818	0.71	92.9	72.7	80.6	<0.001
	$NEF_{70\ keV}$	0.834	0.203	85.7	81.8	83.3	<0.001
	λ	0.760	3.293	64.3	77.3	72.2	0.002
	NZeff	0.732	0.773	100.0	40.9	63.9	0.006
	NIC	0.841	0.2	92.9	77.3	83.3	<0.001

P<0.05 indicates statistical significance. ROC, receiver operating characteristic; AUC, area under the curve; $\Delta_{40\ keV/70\ keV}$, attenuation difference of the solitary pulmonary nodule between the 40 keV/70 keV and virtual noncontrast; HU, Hounsfield unit; $\Delta_{S\text{-}A(40\ keV)}$, attenuation difference between the solitary pulmonary nodule in the 40 keV/70 keV and arterial enhancement; $CER_{40\ keV/70\ keV}$, contrast enhancement ratio of the 40 keV/70 keV; $SAR_{40\ keV/70\ keV}$, solitary pulmonary nodule in the 40 keV/70 keV to arterial enhancement ratio; $NEF_{40\ keV/70\ keV}$, normalized arterial enhancement fraction in 40 keV/70 keV; λ, slope of the spectral attenuation curve; NZeff, normalized effective atomic number; NIC, normalized iodine concentration.

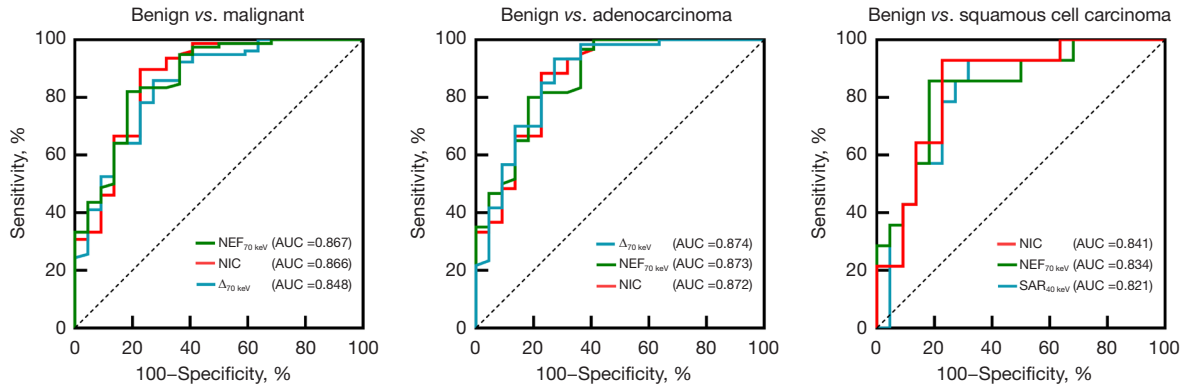

Figure 3 Three-parameter analysis of higher ROC curves for differentiating different pulmonary nodule pathological types. $NEF_{70\ keV}$, normalized arterial enhancement fraction in the 70 keV; AUC, area under the curve; NIC, normalized iodine concentration; $\Delta_{70\ keV}$, attenuation difference of the solitary pulmonary nodule between the 70 keV and virtual noncontrast; $SAR_{40\ keV}$, solitary pulmonary nodule in the 40 keV to arterial enhancement ratio; ROC, receiver operating characteristic.

Table 5 Repeatability of multiparameter measurements between observers

Parameters	ICC (95% CI)
$\Delta_{40\ keV}$	0.981 (0.989–0.967)
$\Delta_{70\ keV}$	0.980 (0.966–0.989)
$\Delta_{S\text{-}A(40\ keV)}$	0.986 (0.975–0.992)
$\Delta_{S\text{-}A(70\ keV)}$	0.995 (0.992–0.997)
$CER_{40\ keV}$	0.856 (0.759–0.915)
$CER_{70\ keV}$	0.877 (0.792–0.928)
$SAR_{40\ keV}$	0.990 (0.983–0.994)
$SAR_{70\ keV}$	0.978 (0.962–0.988)
$NEF_{40\ keV}$	0.987 (0.978–0.993)
$NEF_{70\ keV}$	0.986 (0.976–0.992)
λ	0.957 (0.925–0.975)
NZeff	0.984 (0.971–0.991)
NIC	0.996 (0.993–0.998)

ICC, intraclass correlation coefficient; CI, confidence interval; $\Delta_{40\ keV/70\ keV}$ attenuation difference of the solitary pulmonary nodule between the 40 keV/70 keV and virtual noncontrast; $\Delta_{S\text{-}A(40\ keV/70\ keV)}$, attenuation difference between the solitary pulmonary nodule in the 40 keV/70 keV and arterial enhancement; $CER_{40\ keV/70\ keV}$, contrast enhancement ratio of the 40 keV/70 keV; $SAR_{40\ keV/70\ keV}$, solitary pulmonary nodule in the 40 keV/70 keV to arterial enhancement ratio; $NEF_{40\ keV/70\ keV}$, normalized arterial enhancement fraction in the 40 keV/70 keV; λ, slope of the spectral attenuation curve; NZeff, normalized effective atomic number; NIC, normalized iodine concentration.

compounds or mixtures of various materials and characterizes tissue composition. In our study, Zeff values were higher for malignant pulmonary nodules than for benign pulmonary nodules, possibly because malignant nodules have abundant densely packed tumor cells with a higher nuclear-to-cytoplasmic ratio (31). In this regard, there is a paucity of studies on the Zeff of pulmonary nodules.

As the main component of contrast agents, iodine directly reflects blood flow and distribution in intravascular and extracellular spaces. IC maps are generally considered to enable assessment of the number and blood flow of blood vessels supplying pulmonary nodules. Standardized NIC parameters with aortic IC minimize the effects of hemodynamic factors on absolute enhancement of lesions between different individuals, thereby increasing comparability between different cases and specificity of iodine-related NICs compared to other indicators. Our study demonstrated that the NIC of malignant nodules was significantly higher than that of benign nodules. Compared to benign nodules, malignant nodules required a greater blood supply to provide tumor cells with more essential nutrients and oxygen, thereby resulting in rapid growth that manifested as a significant increase in microvessels and abundant blood supply.

ROC curve analysis revealed relatively high AUCs (0.709–0.867) of the relevant parameters for discriminating benign and malignant nodules. The three parameters with the highest AUC distributions were $NEF_{70\ keV}$, NIC,

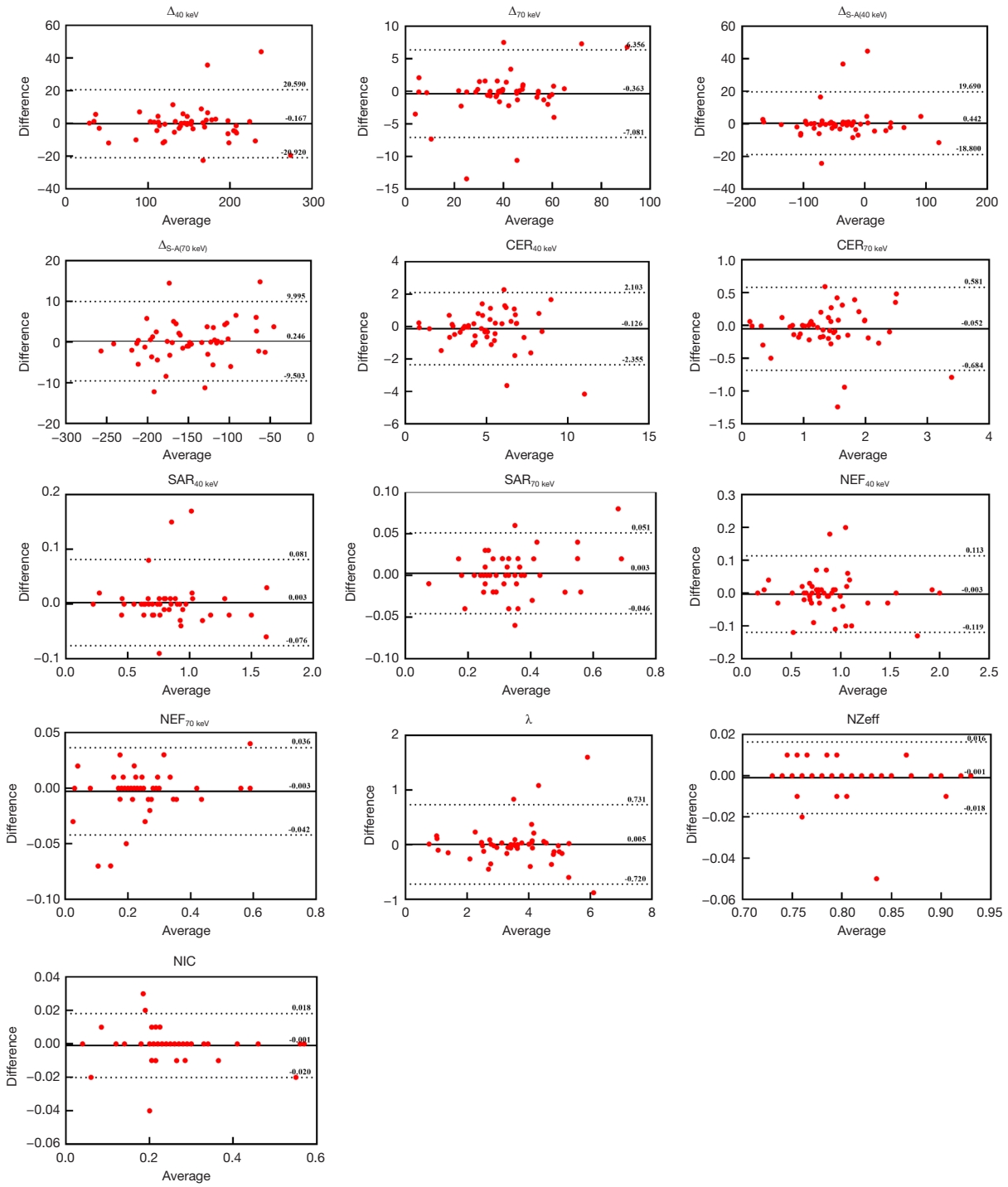

Figure 4 Bland-Altman plots of interobserver differences in spectral CT-derived parameters. $\Delta_{40\ keV/70\ keV}$, attenuation difference of the solitary pulmonary nodule between the 40 keV/70 keV and virtual noncontrast; $\Delta_{S\text{-}A(40\ keV/70\ keV)}$, attenuation difference between the solitary pulmonary nodule in the 40 keV/70 keV and arterial enhancement; $CER_{40\ keV/70\ keV}$, contrast enhancement ratio of the 40 keV/70 keV; $SAR_{40\ keV/70\ keV}$, solitary pulmonary nodule in the 40 keV/70 keV to arterial enhancement ratio; $NEF_{40\ keV/70\ keV}$, normalized arterial enhancement fraction in the 40 keV/70 keV; λ, slope of the spectral attenuation curve; NZeff, normalized effective atomic number; NIC, normalized iodine concentration; CT, computed tomography.

and $\Delta_{70\ keV}$ (AUCs: 0.867, 0.866, and 0.848, respectively). For previous conventional CT, cut-off values of contrast-enhanced CT for discriminating benign and malignant nodules were set at 15–30 Hounsfield units (HUs) (12,32,33). Our cut-off value was almost the same as that of Yi *et al.* (32) (33.3 and 30 HU, respectively), with a net enhancement of ≥30 HU as the cut-off for distinguishing benign from malignant nodules. The sensitivity, specificity, and accuracy for malignant nodules were 99%, 54%, and 78%, respectively. In a study by Swensen *et al.* (12) with 15 HU as the threshold, the sensitivity, specificity, and accuracy were 98%, 58%, and 77% respectively. This discrepancy may be related to the injection rate, total volume, and acquisition time of the contrast medium. The mean difference in the CT number of SPNs on non-enhanced weighted mean images and virtual non-enhanced images was 4.3 HU. Moreover, the attenuation value of pulmonary nodules on real plain images was similar to that on virtual plain images. In routine practice, virtual non-enhanced image reconstruction can replace additional non-enhanced CT scans to reduce their radiation dose (34). As 70 keV is equivalent to conventional CT values, we conjecture that $\Delta_{70\ keV}$ is equivalent to enhanced CT values. In our study, $\Delta_{70\ keV}$ had a sensitivity, specificity, and accuracy of 85.9%, 72.7%, and 83.0%, respectively, for identifying benign and malignant nodules. The NIC cut-off for distinguishing benign from malignant tumors was 0.2, which is consistent with previous findings (14,16). Wen *et al.* (14) obtained NIC cut-offs of 0.13 and 0.31 using 25-s and 60-s spectral CT enhanced scans. Our cut-offs using 50-s enhanced scans fell well within this range. Zhang *et al.* (16) reported NIC cut-offs of 0.21 and 0.30 for 35-s and 90-s enhanced scans, respectively, and our values also fell within this range. In our study, no significant difference was observed between the AUC curves of $NEF_{70\ keV}$, NIC, and $\Delta_{70\ keV}$. Although the AUC of the $NEF_{70\ keV}$ parameter was the highest, the sensitivity and accuracy were lower than those of NIC. Hence, we considered NIC the most effective potential parameter.

The present study also demonstrated that contrast-enhanced CT-derived multiparameters performed well for differentiating benign tumors from adenocarcinoma and squamous cell carcinoma. However, no significant differences were observed in quantitative multiparameters between adenocarcinoma and squamous cell carcinoma, with the exception of $CER_{70\ keV}$. This is in accordance with some previous reports but not with others (35,36). Theoretically, the neovascularization of adenocarcinoma should be higher than that of squamous cell carcinoma, and the distribution should be relatively uniform, with less necrosis and hemorrhage. Compared to adenocarcinomas, squamous cell carcinomas are larger and more likely to invade blood vessels. The tumor blood vessels of squamous cell carcinoma are more likely to break, shrink, and block due to accumulation and growth, eventually leading to necrosis. Moreover, the degree of enhancement is lower than that of adenocarcinoma. We speculate that this may be related to the following factors. First, we examined SPNs rather than pulmonary masses, as reported in previous studies. Given the small size of the lesions investigated in our study, even squamous cell carcinoma may not have exhibited obvious necrosis. In addition, our software for delineating lesions automatically avoided areas with obvious necrosis and enhancement; therefore, the ROI was predominantly located in lesions with uniform density. This may have resulted in a degree of measurement bias in the results, consistent with the theory of Li *et al.* (35). In addition, a relationship with a smaller number of squamous cell carcinomas or scanning time has been proposed (36).

Consistent with previous studies, our study demonstrated good interobserver agreement for spectral CT multiparameters measured using a semiautomated full-volume method, indicating good reproducibility and stability for lung nodule assessment (19). Spectral CT parameters in this study were derived from the entire volume of the lesion. However, in most previous studies, only parameter values from 1 or several manually drawn ROIs were used due to technical or software limitations. This approach was unable to reflect the heterogeneity and full information of lesions and precluded a complete characterization of whole tumor biology, which may have impacted the accuracy of delineating lesions (37). A study by Gierada *et al.* (19) reported that nodule volumes obtained using semiautomated CT volume methods had consistently high interobserver agreement compared with manual or semi-automated nodule diameters. These results were consistent with the expectations that volume measurements were more consistent and less variable compared with size measurements of lung nodules and tumors (19).

Our study had several limitations. First, it was a single-center retrospective study with a relatively small sample size. Although the sample size of previous studies on SPNs has rarely exceeded 100, larger sample sizes and multicenter validation are warranted. Second, in our study, only 13 parameters obtained from venous phase scan images were used in a single phase to reduce radiation dose. Several

studies (14,23) have used dual-phases (arterial and venous phase scans), and we intend to perform dual-phase scanning in the future. However, some studies (14,23) have reported that several parameters such as IC/slope in the venous phase may be superior to those in the arterial phase. Third, our radiologists had experience in evaluating benign pulmonary nodules, and the number of benign pulmonary nodules that were difficult to identify and ended being treated surgically was low. Fourth, we did not include morphological features in this study, because we focused predominantly on the evaluation of pulmonary nodules using quantitative parameters. In this regard, we plan to further investigate the combined features of morphological and quantitative parameters in the future. Finally, our study was performed using a dual-source CT device, and the application of this scanning principle to different types of dual-energy scanners warrants validation in future multicentre large-sample studies.

Conclusions

In conclusion, our findings demonstrate the potential value of spectral CT-related parameters extracted using a full-volume approach for evaluating pulmonary nodules with satisfactory diagnostic performance and reproducibility.

Acknowledgments

Funding: This work was supported by the Nanjing Medical University Imaging Elite Talents Project (No. 320.1140.2022.0510.005) and the Scientific Research Project of Jiangsu Provincial Health Commission (No. Z2022075).

Footnote

Reporting Checklist: The authors have completed the STARD reporting checklist. Available at https://qims.amegroups.com/article/view/10.21037/qims-22-979/rc

Conflicts of Interest: All authors have completed the ICMJE uniform disclosure form (available at https://qims.amegroups.com/article/view/10.21037/qims-22-979/coif). The authors have no conflicts of interest to declare.

Ethical Statement: The authors are accountable for all aspects of the work in ensuring that questions related to the accuracy or integrity of any part of the work are appropriately investigated and resolved. The study was conducted in accordance with the Declaration of Helsinki (as revised in 2013). The Institutional Ethics Committee of Jiangsu Cancer Hospital approved this study, and individual consent for this retrospective analysis was waived.

References

1. Siegel RL, Miller KD, Jemal A. Cancer statistics, 2015. CA Cancer J Clin 2015;65:5-29.
2. Sung H, Ferlay J, Siegel RL, Laversanne M, Soerjomataram I, Jemal A, Bray F. Global Cancer Statistics 2020: GLOBOCAN Estimates of Incidence and Mortality Worldwide for 36 Cancers in 185 Countries. CA Cancer J Clin 2021;71:209-49.
3. Weir-McCall JR, Joyce S, Clegg A, MacKay JW, Baxter G, Dendl LM, Rintoul RC, Qureshi NR, Miles K, Gilbert FJ. Dynamic contrast-enhanced computed tomography for the diagnosis of solitary pulmonary nodules: a systematic review and meta-analysis. Eur Radiol 2020;30:3310-23.
4. Ost D, Fein AM, Feinsilver SH. Clinical practice. The solitary pulmonary nodule. N Engl J Med 2003;348:2535-42.
5. Winer-Muram HT. The solitary pulmonary nodule. Radiology 2006;239:34-49.
6. Truong MT, Ko JP, Rossi SE, Rossi I, Viswanathan C, Bruzzi JF, Marom EM, Erasmus JJ. Update in the evaluation of the solitary pulmonary nodule. Radiographics 2014;34:1658-79.
7. Siegelman SS, Khouri NF, Leo FP, Fishman EK, Braverman RM, Zerhouni EA. Solitary pulmonary nodules: CT assessment. Radiology 1986;160:307-12.
8. Khouri NF, Meziane MA, Zerhouni EA, Fishman EK, Siegelman SS. The solitary pulmonary nodule. Assessment, diagnosis, and management. Chest 1987;91:128-33.
9. Gould MK, Ananth L, Barnett PG; Veterans Affairs SNAP Cooperative Study Group. A clinical model to estimate the pretest probability of lung cancer in patients with solitary

pulmonary nodules. Chest 2007;131:383-8.
10. Aberle DR, Adams AM, Berg CD, Black WC, Clapp JD, Fagerstrom RM, Gareen IF, Gatsonis C, Marcus PM, Sicks JD. Reduced lung-cancer mortality with low-dose computed tomographic screening. N Engl J Med 2011;365:395-409.
11. Erasmus JJ, Connolly JE, McAdams HP, Roggli VL. Solitary pulmonary nodules: Part I. Morphologic evaluation for differentiation of benign and malignant lesions. Radiographics 2000;20:43-58.
12. Swensen SJ, Viggiano RW, Midthun DE, Müller NL, Sherrick A, Yamashita K, Naidich DP, Patz EF, Hartman TE, Muhm JR, Weaver AL. Lung nodule enhancement at CT: multicenter study. Radiology 2000;214:73-80.
13. Deniffel D, Sauter A, Fingerle A, Rummeny EJ, Makowski MR, Pfeiffer D. Improved differentiation between primary lung cancer and pulmonary metastasis by combining dual-energy CT-derived biomarkers with conventional CT attenuation. Eur Radiol 2021;31:1002-10.
14. Wen Q, Yue Y, Shang J, Lu X, Gao L, Hou Y. The application of dual-layer spectral detector computed tomography in solitary pulmonary nodule identification. Quant Imaging Med Surg 2021;11:521-32.
15. Gao L, Lu X, Wen Q, Hou Y. Added value of spectral parameters for the assessment of lymph node metastasis of lung cancer with dual-layer spectral detector computed tomography. Quant Imaging Med Surg 2021;11:2622-33.
16. Zhang Y, Cheng J, Hua X, Yu M, Xu C, Zhang F, Xu J, Wu H. Can Spectral CT Imaging Improve the Differentiation between Malignant and Benign Solitary Pulmonary Nodules? PLoS One 2016;11:e0147537.
17. Wu L, Cao G, Zhao L, Tang K, Lin J, Miao S, Lin T, Sun J, Zheng X. Spectral CT Analysis of Solitary Pulmonary Nodules for Differentiating Malignancy from Benignancy: The Value of Iodine Concentration Spatial Distribution Difference. Biomed Res Int 2018;2018:4830659.
18. Azour L, Ko JP, O'Donnell T, Patel N, Bhattacharji P, Moore WH. Combined whole-lesion radiomic and iodine analysis for differentiation of pulmonary tumors. Sci Rep 2022;12:11813.
19. Gierada DS, Rydzak CE, Zei M, Rhea L. Improved Interobserver Agreement on Lung-RADS Classification of Solid Nodules Using Semiautomated CT Volumetry. Radiology 2020;297:675-84.
20. Ma Z, Liang C, Huang Y, He L, Liang C, Chen X, Huang X, Xiong Y, Liu Z. Can lymphovascular invasion be predicted by preoperative multiphasic dynamic CT in patients with advanced gastric cancer? Eur Radiol 2017;27:3383-91.
21. Yin XD, Huang WB, Lü CY, Zhang L, Wang LW, Xie GH. A preliminary study on correlations of triple-phase multi-slice CT scan with histological differentiation and intratumoral microvascular/lymphatic invasion in gastric cancer. Chin Med J (Engl) 2011;124:347-51.
22. Komori M, Asayama Y, Fujita N, Hiraka K, Tsurumaru D, Kakeji Y, Honda H. Extent of arterial tumor enhancement measured with preoperative MDCT gastrography is a prognostic factor in advanced gastric cancer after curative resection. AJR Am J Roentgenol 2013;201:W253-61.
23. Deng L, Zhang G, Lin X, Han T, Zhang B, Jing M, Zhou J. Comparison of Spectral and Perfusion Computed Tomography Imaging in the Differential Diagnosis of Peripheral Lung Cancer and Focal Organizing Pneumonia. Front Oncol 2021;11:690254.
24. Zhang X, Zheng C, Yang Z, Cheng Z, Deng H, Chen M, Duan X, Mao J, Shen J. Axillary Sentinel Lymph Nodes in Breast Cancer: Quantitative Evaluation at Dual-Energy CT. Radiology 2018;289:337-46.
25. Wang X, Liu D, Zeng X, Jiang S, Li L, Yu T, Zhang J. Dual-energy CT quantitative parameters for the differentiation of benign from malignant lesions and the prediction of histopathological and molecular subtypes in breast cancer. Quant Imaging Med Surg 2021;11:1946-57.
26. Li H, Wang H, Chen F, Gao L, Zhou Y, Zhou Z, Huang J, Xu L. Detection of axillary lymph node metastasis in breast cancer using dual-layer spectral computed tomography. Front Oncol 2022;12:967655.
27. Ha T, Kim W, Cha J, Lee YH, Seo HS, Park SY, Kim NH, Hwang SH, Yong HS, Oh YW, Kang EY, Kim C. Differentiating pulmonary metastasis from benign lung nodules in thyroid cancer patients using dual-energy CT parameters. Eur Radiol 2022;32:1902-11.
28. Li LM, Feng LY, Chen XH, Liang P, Li J, Gao JB. Gastric heterotopic pancreas and stromal tumors smaller than 3 cm in diameter: clinical and computed tomography findings. Cancer Imaging 2018;18:26.
29. Li Y, Su H, Yang L, Yue M, Wang M, Gu X, Dai L, Wang X, Su X, Zhang A, Ren J, Shi G. Can lymphovascular invasion be predicted by contrast-enhanced CT imaging features in patients with esophageal squamous cell carcinoma? A preliminary retrospective study. BMC Med Imaging 2022;22:93.
30. Zegadło A, Żabicka M, Kania-Pudło M, Maliborski A, Różyk A, Sośnicki W. Assessment of Solitary Pulmonary Nodules Based on Virtual Monochrome Images and Iodine-Dependent Images Using a Single-Source Dual-

Energy CT with Fast kVp Switching. J Clin Med 2020;9:2514.
31. Shen H, Yuan X, Liu D, Huang Y, Wang Y, Jiang S, Zhang J. Multiparametric dual-energy CT for distinguishing nasopharyngeal carcinoma from nasopharyngeal lymphoma. Eur J Radiol 2021;136:109532.
32. Yi CA, Lee KS, Kim EA, Han J, Kim H, Kwon OJ, Jeong YJ, Kim S. Solitary pulmonary nodules: dynamic enhanced multi-detector row CT study and comparison with vascular endothelial growth factor and microvessel density. Radiology 2004;233:191-9.
33. Cha MJ, Lee KS, Kim HS, Lee SW, Jeong CJ, Kim EY, Lee HY. Improvement in imaging diagnosis technique and modalities for solitary pulmonary nodules: from ground-glass opacity nodules to part-solid and solid nodules. Expert Rev Respir Med 2016;10:261-78.
34. Chae EJ, Song JW, Seo JB, Krauss B, Jang YM, Song KS. Clinical utility of dual-energy CT in the evaluation of solitary pulmonary nodules: initial experience. Radiology 2008;249:671-81.
35. Li X, Meng X, Ye Z. Iodine quantification to characterize primary lesions, metastatic and non-metastatic lymph nodes in lung cancers by dual energy computed tomography: An initial experience. Eur J Radiol 2016;85:1219-23.
36. Zhang Z, Zou H, Yuan A, Jiang F, Zhao B, Liu Y, Chen J, Zuo M, Gong L. A Single Enhanced Dual-Energy CT Scan May Distinguish Lung Squamous Cell Carcinoma From Adenocarcinoma During the Venous phase. Acad Radiol 2020;27:624-9.
37. Li M, Zhang L, Tang W, Jin YJ, Qi LL, Wu N. Identification of epidermal growth factor receptor mutations in pulmonary adenocarcinoma using dual-energy spectral computed tomography. Eur Radiol 2019;29:2989-97.

Cite this article as: Liu K, Wang M, Xu Y, Chen Q, Li K, Zhang L, Xie X, Shen W. Value of spectral computed tomography-derived quantitative parameters based on full volume analysis in the diagnosis of benign/malignant and pathological subtypes of solitary pulmonary nodules. Quant Imaging Med Surg 2023;13(6):3827-3840. doi: 10.21037/qims-22-979

